Complex Capacitance Scaling in Ionic Liquids-Filled Nanopores

Peng Wu,[†] Jingsong Huang,[‡] Vincent Meunier,[§] Bobby G. Sumpter,[‡] and Rui Qiao[†,*]

[†]Department of Mechanical Engineering, Clemson University, Clemson, South Carolina 29634-0921, United States, [‡]Center for Nanophase Materials Sciences and Computer Science and Mathematics Division, Oak Ridge National Laboratory, Bethel Valley Road, Oak Ridge, Tennessee 37831-6367, United States, and [§]Department of Physics, Applied Physics, and Astronomy, Rensselaer Polytechnic Institute, Troy, New York 12180-3590, United States

ABSTRACT

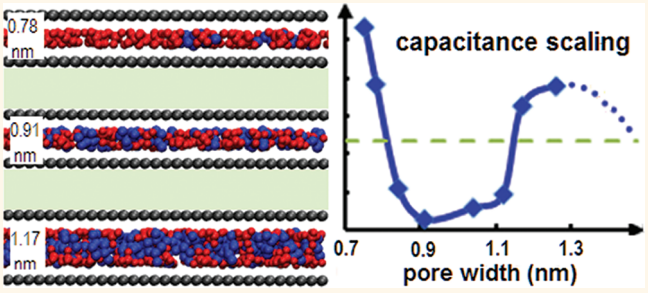

Recent experiments have shown that the capacitance of subnanometer pores increases anomalously as the pore width decreases, thereby opening a new avenue for developing supercapacitors with enhanced energy density. However, this behavior is still subject to some controversy since its physical origins are not well understood. Using atomistic simulations, we show that the capacitance of slit-shaped nanopores in contact with room-temperature ionic liquids exhibits a U-shaped scaling behavior in pores with widths from 0.75 to 1.26 nm. The left branch of the capacitance scaling curve directly corresponds to the anomalous capacitance increase and thus reproduces the experimental observations. The right branch of the curve indirectly agrees with experimental findings that so far have received little attention. The overall U-shaped scaling behavior provides insights on the origins of the difficulty in experimentally observing the pore-width-dependent capacitance. We establish a theoretical framework for understanding the capacitance of electrical double layers in nanopores and provide mechanistic details into the origins of the observed scaling behavior. The framework highlights the critical role of "ion solvation" in controlling pore capacitance and the importance of choosing anion/cation couples carefully for optimal energy storage in a given pore system.

KEYWORDS: supercapacitor · electrical double layer · room-temperature ionic liquids · anomalous enhancement · nanopores · transmission line model

Supercapacitors store electrical energy physically in electrical double layers (EDLs) at the electrode/electrolyte interface.[1] Despite their high power density and extraordinary cyclability, the widespread deployment of supercapacitors is limited by their moderate energy density. The current surge in interest in supercapacitors is driven by recent breakthroughs in developing novel electrode materials and electrolytes that promise to significantly improve their energy density.[2−6] In particular, a group of experiments showed that the area-normalized capacitance (or specific capacitance, hereafter referred to as capacitance) of subnanometer pores filled with organic or room-temperature ionic liquid (RTIL) electrolytes increases anomalously as the pore width decreases.[6−8] These findings challenge the long-held presumption that subnanometer pores are too small to contribute to energy storage, and suggest that nonclassical behaviors of EDLs emerge in subnanometer pores.

The validity of the anomalous capacitance scaling in subnanometer pores has been challenged by recent experimental studies,[9] in which the capacitances were found to be nearly pore-width independent for pores from 0.7 to 15 nm. The sharp contrast in the observed capacitance scalings was ascribed to the discrepancy in the specific surface area (used for determining the specific capacitance) probed by different methods.[9] The debate about anomalous capacitance is in part fueled by the absence of a complete theoretical description of all the intricate processes taking place at the nanoscale. Along that front, the anomalous capacitance enhancement in subnanometer pores was first described using a heuristic model that assumes that counterions form a wire in the center of a cylindrical pore (or a single layer in the center of a slit-shaped pore).[10,11] Among the recent atomistic simulations of EDLs in nanopores,[12−15] molecular dynamics (MD) simulations of carbon nanotubes (CNTs) filled with RTILs have shown a capacitance increase with decreasing CNT diameter in the range of 2.0 to 0.9 nm.[16] However, the polarizability of the nanotube wall was neglected and the computed capacitances were ~10 fold smaller than experimental values. Recently, a model that takes into account the polarizability

* Address correspondence to rqiao@clemson.edu.

Received for review August 24, 2011 and accepted October 21, 2011.

Published online October 21, 2011
10.1021/nn203260w

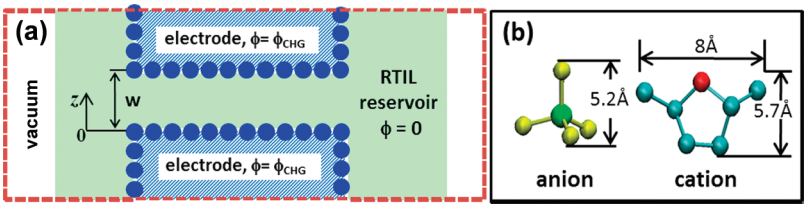

Figure 1. (a) A schematic of the simulation system featuring a slit-shaped nanopore in equilibrium with a RTIL reservoir. The electrode features an equi-potential surface that carries a net charge that is balanced by ions inside the simulation box (denoted by the red dashed line). (b) Schematics of the semicoarse grained model for the cation and the anion. The red sphere in the cation and the green sphere in the anion denote the atoms which carry charges of $+e$ and $-e$, respectively.

of a pore wall showed that the screening of electrostatic interactions and the negative self-energy of ions in pores lead to a superionic state.[17] This model and subsequent Monte Carlo (MC) simulations[18] also reproduced the anomalous capacitance enhancement in subnanometer pores observed experimentally. Despite this agreement, an important difference exists: comparison was made between the experimentally measured *integral* capacitance C_{int} at a potential drop of ϕ_w from an electrode to bulk electrolyte and the theoretically predicted *differential* capacitance C_{diff} at $\phi_w = 0$ V. Using the data presented in the MC simulations,[18] one can show that, for a $\phi_w = 1.5$ V (which can be justified, assuming a symmetric capacitor, for an experimental potential drop of 3 V between the two electrodes[7]), C_{int} increases as the pore width decreases from 1.2 to 1.0 nm but *decreases* as the pore width further decreases, which disagrees with the experimental trend. The experimental trend of C_{int} is recovered if $\phi_w < 1.0$ V.

In this study we use MD simulations to investigate EDLs in slit-shaped nanopores with polarizable walls in equilibrium with RTILs. Our simulations reproduce the anomalous capacitance enhancement when the pore width reduces below a critical value, but also reveal that capacitance increases as the pore width increases beyond another critical value. We provide mechanistic insights into these scaling behaviors by delineating the relation between the structure and the capacitance of the EDLs in these pores. We show that the EDLs inside subnanometer pores filled with RTILs represent a new capacitor regime in which the ubiquitously used transmission-line model for supercapacitors fails qualitatively.

RESULTS AND DISCUSSION

Figure 1a shows a schematic of the MD system that consists of a slit-shaped pore in contact with a reservoir of RTILs. The entire electrode surface (the horizontal pore walls and the vertical walls blocking the RTIL reservoir) is modeled as an equi-potential surface with a net charge. The magnitude of surface charge and electrical potential of the pore walls was not directly controlled, but determined from the ion distribution obtained in the MD simulations (see Methods). Ions were modeled using semicoarse grained models that (1) resolve their geometrical anisotropy and van der Waals interactions, which are important in determining EDL capacitance,[19] and (2) assign the charge of each ion to one of its atoms (Figure 1b and Methods). These models were adopted in the spirit of the hard sphere model[18] which has been shown to capture key features of EDLs in nanopores. Simulations in which the charge of each ion was distributed on its multiple atoms yielded qualitatively similar results, in agreement with our prior finding that charge delocalization plays a relatively unimportant role in determining the thermodynamic properties of EDLs.[19] We note that, however, charge delocalization plays a key role in determining dynamics of RTILs. Hence caution must be used if the present RTIL model is to be used to study EDL dynamics.

TABLE 1. Surface Charge Density (σ) and Electrical Potential (ϕ) in the qPZC and CHG Systems for Various Nanopores. The Electrical Potential in Bulk RTILs Is Taken as Zero

	qPZC system		CHG system		
pore width W (nm)	σ_{qPZC} (C/m^2)	ϕ_{qPZC} (V)	σ_{CHG} (C/m^2)	ϕ_{CHG} (V)	$\Delta\phi$ (V)
0.75	−0.007	0.117	0.172	1.693	1.576
0.78	−0.005	0.010	0.150	1.602	1.592
0.84	−0.003	−0.035	0.118	1.735	1.771
0.91	−0.001	−0.138	0.108	1.584	1.721
1.04	0.006	−0.266	0.115	1.445	1.711
1.12	0.007	−0.283	0.121	1.373	1.656
1.17	−0.002	−0.084	0.148	1.672	1.757
1.26	−0.005	−0.028	0.157	1.621	1.649

To compute the integral capacitance, two systems were simulated for each pore width: in a quasi-potential of zero charge (qPZC) system, the net charge of the entire electrode was zero; in a charged (CHG) system, the net charge of the entire electrode was positive, and the anion sketched in Figure 1b serves as the counterion. The potentials of the pore wall with respect to the RTIL reservoir in these two systems were determined to be ϕ_{qPZC} and ϕ_{CHG}, respectively. The surface charge densities of the pore wall were determined as σ_{qPZC} and σ_{CHG}, respectively. ϕ_{qPZC}, ϕ_{CHG}, σ_{qPZC}, and σ_{CHG} for the various pores studied are summarized in Table 1. In the qPZC systems, σ_{qPZC} deviates slightly from zero due to the different affinity of ions to the horizontal pore wall and the open vertical walls. The integral capacitance of each pore was computed using $C_{int} = \Delta\sigma/\Delta\phi$,

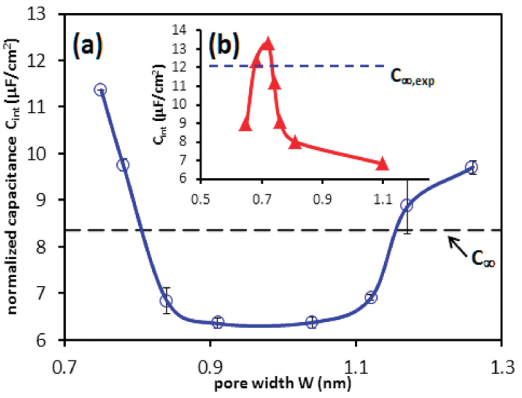

Figure 2. (a) Variation of EDL capacitance from MD simulations in pores with center-to-center width from W = 0.75–1.26 nm. C_∞ denotes the capacitance of an open planar electrode. (b) Variation of EDL capacitance in pores filled with EMI-TFSI electrolye reported in ref 7. The experimental capacitance, $C_{\infty,exp}$, was measured on planar glassy carbon electrodes in the same electrolyte.[20] The statistical error for the 1.17 nm pore is relatively large because ion diffusion in this pore is very slow (due to the nearly crystal-like packing inside the neutral pore), which renders simulation difficult.

where $\Delta\sigma = \sigma_{CHG} - \sigma_{qPZC}$ is the increase of pore surface charge density as the pore is electrified by $\Delta\phi = \phi_{CHG} - \phi_{qPZC}$ volts. $\Delta\phi$ of all pores studied is within 0.1 V from the target value of 1.68 V (*cf.* Table 1), which is similar to the experimental potential.[7] Since $\sigma_{CHG} \gg \sigma_{qPZC}$ and $\sigma_{qPZC} \approx 0$ in all pores, the computed capacitance approximates well the integral capacitance defined by $C_{int} = \sigma_{CHG}/(\phi_{CHG} - \phi_{PZC})$,[21] where ϕ_{PZC} is the surface potential of a neutral pore.

Capacitance Scaling. Figure 2a shows the variation of capacitance (C_{int}) with the *center-to-center* width (W) of the pores, where a U-shaped C_{int}–W curve is observed. The trend revealed by the left branch of the C_{int}–W curve agrees with that reported experimentally (see Figure 2b): it simultaneously captures the sharp increase of C_{int} as W decreases from 0.91 to 0.75 nm and its slight change as W decreases from 1.12 to 0.91 nm; the latter was not found by a prior analytical model.[10] We note that the pore width reported in ref 7 is most likely the "accessible width", which is about one van der Waals diameter (~0.3 nm) smaller than the "center-to-center width" used in Figure 2a. If C_{int} in Figure 2a is plotted against the "accessible width", it would shift toward a smaller pore width by ~0.3 nm, suggesting that the capacitance enhancement would appear in a narrower pore width range (0.45–0.61 nm) than experiments (0.7–0.8 nm).[7] Such a difference can be attributed to the fact that the counterion in our simulation (~0.52 nm in diameter) is smaller than that used in the experiments (the largest dimension of both anions and cations is ~0.8 nm).[7] Nevertheless, the trend of the capacitance scaling, the focus of the present study, bears a close resemblance to the experimental one.

The sharp increase of C_{int} with W ranging from 1.12 to 1.26 nm has not been directly reported experimentally but is indirectly supported by measurements. Figure 2b shows that the experimental capacitance of a 1.1 nm pore is ~7 μF/cm^2,[7] whereas the experimental capacitance of planar electrodes made of glassy carbon in the same electrolyte is ~12 μF/cm^2.[20] This difference implies that the capacitance of pores larger than 1.1 nm should increase toward the planar surface value with increasing W. Figure 2a does show that the capacitance increases with increasing pore width but it does not approach C_∞ in an asymptotic way since the capacitance in a 1.26 nm pore is higher than C_∞. This suggests that as the pore width further increases, capacitance will decrease again and eventually reach C_∞. How C_∞ is reached as W increases, for example, by a damped oscillation or by a smooth decay, is an interesting question, and may be pursued in future studies. However, we expect the capacitance will not vary significantly in wider pores based on the insights obtained from the analysis below. Specifically, as will be shown later, the pore capacitance is controlled primarily by the change of "ion solvation" in pores as the pore becomes electrified (the "ion solvation" in RTILs refers to the electrostatic and van der Waals interactions between a cation and its surrounding anions (and vice versa). This is qualitatively similar to organic electrolytes consisting of ions solvated by solvent molecules. The quotation marks are removed for later usage of solvation for simplicity). When pore width W increases, the solvation experienced by ions in different pores becomes increasingly similar. Hence the change of their solvation upon pore electrification will not differ significantly as W increases, subsequently resulting in a weaker dependence of capacitance on W. The capacitance scaling trend shown in Figure 2 was also observed in simulations in which the charge of cation and anion was distributed among all their atoms, although the capacitance increases less sharply; e.g., the capacitance enhancement is 20% less sharp compared to data herein as pore size varies from 0.91 to 0.75nm.

The above results suggest that the dependence of the nanopore capacitance on the pore width is more complex than previously expected in experimental and theoretical studies. In view of the ongoing debate on the anomalous capacitance enhancement in subnanometer pores, our results strongly support the existence of the anomalous capacitance enhancement. Additionally, the sharp increase of capacitance over very narrow pore widths (0.75–0.91 nm and 1.12–1.26 nm) and the U-shaped C_{int}–W curve for W < 1.26 nm (and the possibly oscillatory C_{int}–W curve for W > 1.26 nm) indicate that, for the pore-width dependent capacitance to be observed experimentally, it is *essential* that the electrode materials used in experimental characterization feature unimodal and narrow pore-width distribution. When electrodes with multimodal and/or wide pore-width distribution are used, the capacitance variation in different pores can be averaged out. In this regard, we note that most of the electrodes used in ref 9, where the capacitance was found to be

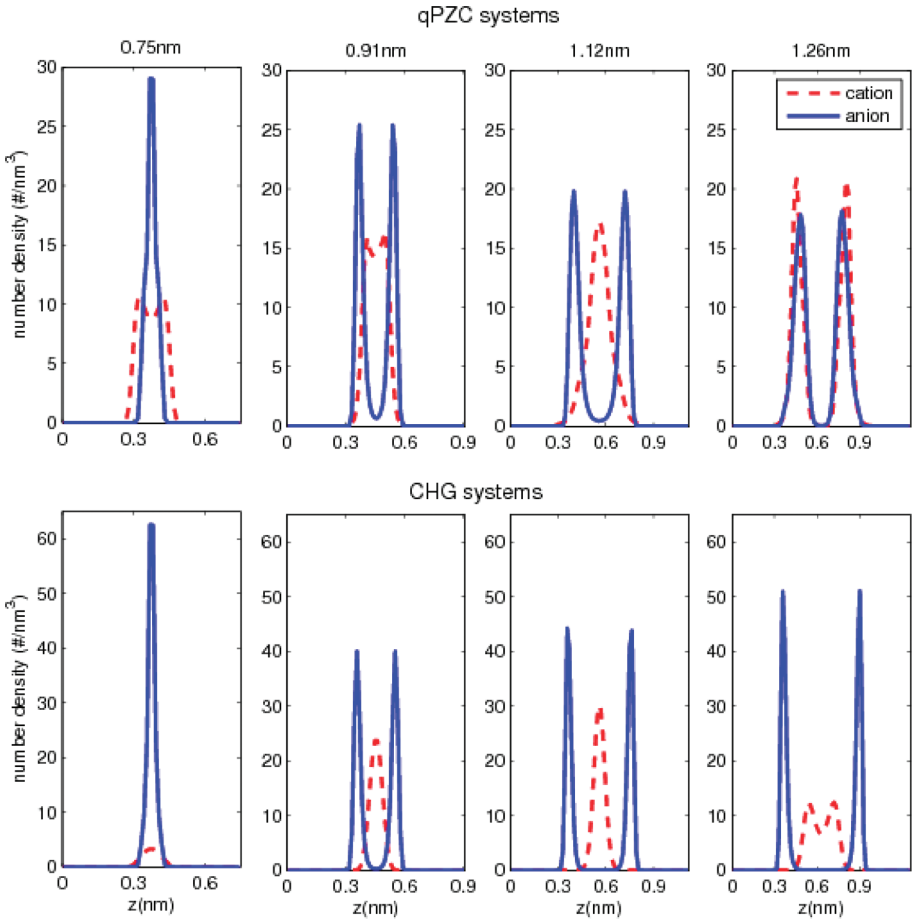

Figure 3. The upper pannels show the ion density in the qPZC systems, and the lower panels show the ion density in the CHG systems. The pore wall surface charge density and surface potential for each system are shown in Table 1. The position of ions is based on the location of their charged atoms.

nearly pore-width independent, are based on activated carbons. Since such electrodes are prone to a relatively wide pore-width distribution, it is possible that the independence of capacitance on pore width observed in those experiments is caused by the averaging effect.

EDL Structure Inside Pores. The capacitance scaling shown in Figure 2a is ultimately controlled by the different EDL structures in various pores. Figure 3 shows the cation and anion density profiles across pores with W = 0.75, 0.91, 1.12, and 1.26 nm in the qPZC system and in the CHG system (density profiles for other pores are given in the Supporting Information). We observe that, when the pore is neutral or nearly neutral, a large amount of ions accumulate inside the pore. In pores with W = 0.75 and 0.78 nm, cations and anions form a monolayer in the pore center, due to the wall confinement. In wider pores, anions always form one layer near each wall, which is an expected behavior for molecules confined in pores wider than twice their diameter. The cation distribution, however, shows more complex behavior: in pores with W = 0.84 and 0.91 nm, they reside rather uniformly across the accessible width of the pore; in pores with W = 1.12 nm, they accumulate in a narrow band near the pore central plane; in pores with W = 1.17 and 1.26 nm, they form a distinct layer near each pore wall. The different cation distributions in these pores are mainly driven by the tendency of cations to maximize their solvation by anions. We computed the solvation number of cations across these pores (*i.e.*, the number of anions within r_1 from a cation, where r_1 is the first local minimum of the cation−anion radial distribution function) and found that its distribution profile resembles the cation density profile. The ion distribution profiles in electrified pores are simpler. In pores with W = 0.75 and 0.78 nm, limited amount of cations (co-ions) and mostly anions (counterions) form a monolayer in the pore center. In wider pores, counterions form two distinct layers, while co-ions accumulate mainly in the pore center.

The observed ion distributions are closely related to the geometry of the ions used here. For example, in neutral pores with W = 1.17 and 1.26 nm, *contact* pairs of cations and anions are positioned side-by-side across the pore.[22] Such crystal-like packing of cations and anions results in strong solvation of these ions, which in turn leads to a distinct layer of cation/anion near each pore wall and significantly slowed ion diffusion inside the pores (the diffusion coefficients of both ions are less than 1/10 of their bulk value). In neutral pores with W = 1.12 nm, however, the pores are too

narrow to accommodate a contact pair of cation and anion positioned across the pore, and cations must reside in the pore center to maximize their solvation. Since ions used in this study are representative of RTILs in which the cation shape is strongly anisotropic and the anion is quasi-spherical, the results obtained here are relevant to this broad class of RTILs.

Physical Origins of Capacitance Scaling in Nanopores. To gain mechanistic insights into the capacitance scaling behavior shown in Figure 2a and its relation with the EDL structure shown in Figure 3, we derive a model for the EDL capacitance. Consider a pore in equilibrium with an RTIL reservoir. Under an electrifying potential ϕ, the pore surfaces acquire a charge density of σ (throughout this work, the electrical potential in reservoir is taken as zero). The electrochemical potential of an ion i inside the pore, $\mu_{i,\text{pore}(\phi,\sigma)}$, is the free energy cost for inserting the ion into the pore, which is equal to its electrochemical potential in the reservoir ($\mu_{i,\infty}$):

$$\begin{aligned}\mu_{i,\,\text{pore}(\phi,\,\sigma)} &= E_{i\rightarrow\text{all}}(\sigma) + \Delta E_{\text{all others}}(\sigma) - T\Delta S(\sigma)\\ &= \mu_{i,\infty}\end{aligned} \tag{1}$$

where the first term on the right-hand side is the interaction energy between the inserted ion and all species in the pore including the walls, and (σ) is used to emphasize that the configuration of all species (including ion i) used to determine $E_{i\rightarrow\text{all}}$ corresponds to the state at which the pore has a surface charge density of σ; the second term is the change of interaction energy between all other species as the ion is inserted into the pore, and it includes the cavitation energy cost when the ions around the inserted ion are separated from each other to generate a cavity to accommodate the inserted ion; the third term stands for entropic effects. Splitting the energy between ion i and all species into an electrostatic part $E^{\text{elec}}_{i\rightarrow\text{all}}(\sigma)$ and a non-electrostatic part $E^{\text{non-elec}}_{i\rightarrow\text{all}}(\sigma)$, we have

$$\begin{aligned}&E^{\text{elec}}_{i\rightarrow\text{all}}(\sigma) + E^{\text{non-elec}}_{i\rightarrow\text{all}}(\sigma) + \Delta E_{\text{all others}}(\sigma) - T\Delta S(\sigma)\\ &\quad= \mu_{i,\infty}\end{aligned} \tag{2}$$

With the use of the superposition principle in electrostatics, the energy of an ion i due to its electrostatic interactions with all species inside a polarizable slit-shaped pore with a surface potential of ϕ is

$$E^{\text{elec}}_{i\rightarrow\text{all}}(\sigma) = q_i\phi + \sum_{j\neq i} E^{\text{elec}}_{i\rightarrow j}(\sigma) + E_{i,\,\text{self}}(\sigma) \tag{3}$$

where q_i is the charge of ion i, j is the index of all ions, $E^{\text{elec}}_{i\rightarrow j}(\sigma)$ is the electrostatic interaction energy between ions i and j given by[17]

$$E^{\text{elec}}_{i\rightarrow j}(\sigma) = \frac{q_iq_j}{\pi\varepsilon_0\varepsilon_r W}\sum_{n=1}^{\infty}\sin\left(\frac{n\pi z_i}{W}\right)\sin\left(\frac{n\pi z_j}{W}\right)K_0\left(\frac{n\pi R_{ij}}{W}\right) \tag{4}$$

where ε_0 and ε_r are the vacuum permittivity and background dielectric constant, respectively; z_i and z_j are the distance of ion i and j from the lower pore wall, respectively; K_0 is the zeroth order modified Bessel function of the second kind, which decreases sharply as its argument increases; R_{ij} is the lateral ion−ion separation, that is, separation between ions i and j in direction parallel to the pore wall; $E_{i,\text{self}}$ is the self-energy of ion i, which depends on the pore width W and ion's position inside the pore.[17,23] Using eqs 2 and 3, we obtain

$$\begin{aligned}\phi = [\mu_{i,\infty} &- \sum_{j\neq i} E^{\text{elec}}_{i\rightarrow j}(\sigma) - E_{i,\,\text{self}}(\sigma) - E^{\text{non-elec}}_{i\rightarrow\text{all}}(\sigma)\\ &- ETS(\sigma)]/q_i\end{aligned} \tag{5}$$

where $ETS(\sigma) = \Delta E_{\text{all others}}(\sigma) - T\Delta S(\sigma)$. Applying eq 5 to an electrified pore (surface potential ϕ; surface charge density σ) and a neutral pore (surface potential ϕ_{PZC}) with the same width, and using $C_{\text{int}} = \sigma/(\phi - \phi_{\text{PZC}})$, we obtain

$$\begin{aligned}C_{\text{int}} = -q_i\sigma/[&\Delta E^{\text{elec}}_{i\rightarrow ions}(0\rightarrow\sigma) + \Delta E^{\text{non-elec}}_{i\rightarrow\text{all}}(0\rightarrow\sigma)\\ &+ \Delta E_{i,\,\text{self}}(0\rightarrow\sigma) + (ETS(\sigma) - ETS(0))]\end{aligned} \tag{6}$$

where $\Delta E^{\text{elec}}_{i\rightarrow\text{all}}(0\rightarrow\sigma) = \sum_{j\neq i}E^{\text{elec}}_{i\rightarrow j}(\sigma) - \sum_{j\neq i}E^{\text{elec}}_{i\rightarrow j}(0)$ is the change in electrostatic interaction energy of an ion i with other ions as the pore surfaces acquire a charge density σ (note that the number of counter/co-ions and their positions inside the pore change accordingly during this process). $\Delta E^{\text{non-elec}}_{i\rightarrow\text{all}}(0\rightarrow\sigma) = E^{\text{non-elec}}_{i\rightarrow\text{all}}(\sigma) - E^{\text{non-elec}}_{i\rightarrow\text{all}}(0)$ and $\Delta E_{i,\text{self}}(0\rightarrow\sigma) = E_{i,\text{self}}(\sigma) - E_{i,\text{self}}(0)$ are the changes in non-electrostatic energy and in self-energy of an ion i as the pore surfaces acquire a charge density σ, respectively. The first three terms in the denominator of eq 6 are expected to dominate over the remaining terms that represent higher order interactions and entropic effects. $\Delta E_{i,\text{self}}(0\rightarrow\sigma)$ is small and can be neglected. Consequently, for the scaling of capacitance, we have

$$\begin{aligned}C_{\text{int}}&\sim q_i/[-\Delta E^{\text{elec}}_{i\rightarrow\text{ions}}(0\rightarrow\sigma)/\sigma - \Delta E^{\text{non-elec}}_{i\rightarrow all}(0\rightarrow\sigma)/\sigma]\\ &\sim q_i/[-\Delta E^{\text{tot}}_{i\rightarrow\text{all}}(0\rightarrow\sigma)/\sigma]\end{aligned} \tag{7}$$

where $\Delta E^{\text{tot}}_{i\rightarrow\text{all}} = \Delta E^{\text{elec}}_{i\rightarrow\text{ions}} + \Delta E^{\text{non-elec}}_{i\rightarrow\text{all}}$. Equation 7 correlates the capacitance of EDLs in a pore with the *variation* of ion energy (and ultimately the *variation* of EDL structure) as the pore is electrified.

To understand the physical meaning of eq 7, we consider a pore electrified by a positive potential ϕ. Here, each cation inside the pore is affected by two factors when the pore becomes electrified: (1) its energy due to the interaction with the pore walls increases by $q_i\phi$, and (2) its energy due to the interaction with others species becomes more negative (and stabilized) when the pore acquires net negative space charge, that is, $\Delta E^{\text{tot}}_{i\rightarrow\text{all}} < 0$. While the first factor tends to drive the cations out of the pore, the second factor tends to hold them inside. Consequently, for each unit negative space charge the pore gains (or, for each unit

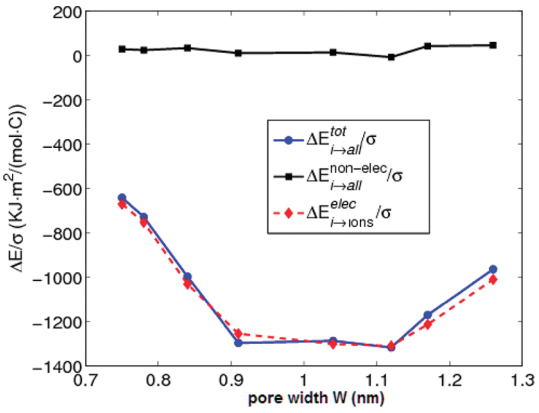

Figure 4. Variation of $\Delta E^{tot}_{i\rightarrow all}(0\rightarrow\sigma)/\sigma$ and its two components in the pores studied. The ion energy in the qPZC system is used to approximate the ion energy in neutral pores.

positive surface charge the pore walls gain), if the energy gain of cations due to their interactions with other species inside the pore is significant, that is, $-\Delta E^{tot}_{i\rightarrow all}/\sigma$ is large, it will be difficult to remove them from the pore. This tends to lead to a small net negative space charge in the pore and accordingly to a small capacitance, as predicted by eq 7. Below we delineate the physical origins of the capacitance scaling shown in Figure 2a by analyzing the energy change of cations inside each pore as it becomes positively electrified. A similar analysis has also been performed for anions but is not shown for brevity.

Figure 4 shows the variation of $\Delta E^{tot}_{i\rightarrow all}(0\rightarrow\sigma)/\sigma$ and its two components for cations. We observe that (1) the scaling of capacitance in these pores can be explained by the scaling of $\Delta E^{tot}_{i\rightarrow all}(0\rightarrow\sigma)/\sigma$ using eq 7, and (2) $\Delta E^{tot}_{i\rightarrow all}(0\rightarrow\sigma)/\sigma$ is dominated by $\Delta E^{elec}_{i\rightarrow ions}(0\rightarrow\sigma)$. The latter observation indicates that, as a pore is electrified, the change of a cation's energy due to the change in its electrostatic interactions with other ions, $\Delta E^{elec}_{i\rightarrow ions}(0\rightarrow\sigma)$, is more important than the change in its non-electrostatic interactions with other species. These observations indicate that $\Delta E^{elec}_{i\rightarrow ions}(0\rightarrow\sigma) + \Delta E^{non\text{-}elec}_{i\rightarrow all}(0\rightarrow\sigma)$ in eq 6 indeed dominates over the term $ETS(\sigma) - ETS(0)$, and eq 7 is justified. They also indicate that we can understand the capacitance scaling in Figure 2a by elucidating the physical origins of the scaling of $\Delta E^{elec}_{i\rightarrow ions}(0\rightarrow\sigma)/\sigma$ shown in Figure 4.

In pores within $0.75 \le W \le 0.91$ nm, $\Delta E^{elec}_{i\rightarrow ions}(0\rightarrow\sigma)/\sigma$ becomes less negative as W decreases, and this is caused by two factors. First, the screening of electrostatic interactions increases as W decreases. As first pointed out in ref 17 and shown in eq 4, the electrostatic interaction between two ions confined in a polarizable pore decreases sharply as R_{ij}/W increases. Consequently, as the same amount of net negative space charge is introduced into a pore by adding anions or removing cations, the energy gain of a cation inside a narrower pore tends to be smaller. Second, the degree of a two-dimensional nature of ion solvation increases as W decreases. As W decreases from 0.91 to 0.75 nm, cations/anions inside the pores are increasingly solvated by their counterparts located near their equator (the line connecting the north and south poles of an ion is assumed to be normal to the pore walls) because of wall confinement. As such, anions introduced into (and the cations removed from) narrower pores during pore electrification tend to have a larger lateral distance R_{ij} from the cations remaining inside the pores, which leads to a less negative $\Delta E^{elec}_{i\rightarrow ions}(0\rightarrow\sigma)/\sigma$ in narrower pores according to eq 4.

In pores within $0.91 < W \le 1.12$ nm, $\Delta E^{elec}_{i\rightarrow ions}(0\rightarrow\sigma)/\sigma$ changes slightly as W changes, and this can be understood as follows. As W decreases from 1.12 to 0.91 nm, the increased screening of electrostatic interactions tends to make $\Delta E^{elec}_{i\rightarrow ions}(0\rightarrow\sigma)/\sigma$ less negative. However, as these pores become positively electrified, the newly added anions can distribute near the north/south pole of the remaining cations in the pore due to two effects: (1) the pores are wide enough to allow three-dimensional solvation of ions, and (2) during pore electrification, cations originally located near neutral walls (interfacial cations) are removed and leave more space for the anions to be added into the pore. Of these effects, the second one is more important in the 0.91 nm pore as there are more interfacial cations in the neutral 0.91 nm pores (see Figure 3). Since a displacement of interfacial cations would decrease the lateral anion−cation distance R_{ij}, the second effect tends to make $\Delta E^{elec}_{i\rightarrow ions}(0\rightarrow\sigma)/\sigma$ more negative as W decreases from 1.12 to 0.91 nm. This effect counteracts the increased screening of electrostatic interactions in narrower pores and the result is that $\Delta E^{elec}_{i\rightarrow ions}(0\rightarrow\sigma)/\sigma$ changes slightly as W decreases from 1.12 to 0.91 nm.

In pores within $1.12 < W \le 1.26$ nm, $\Delta E^{elec}_{i\rightarrow ions}(0\rightarrow\sigma)/\sigma$ becomes less negative as W increases, and this trend is mainly caused by the qualitative change of ion solvation structure as W changes. As shown in Figure 3, in a neutral 1.12 nm pore, cations are located mostly in the center of the pore to maximize their solvation by anions located near the two walls. As the pore walls become positively electrified, the number of anions solvating each cation increases but the solvation structure of these cations remains largely unchanged because they are still located at the pore center. In comparison, the 1.26 nm pore follows a qualitatively different scenario. As shown in Figure 3 and described earlier, when these pores are neutral, cations and anions form contact pairs and are positioned side by side across the pore. Such a solvation structure leads to small lateral separation R_{ij} between a cation and its solvation anions, which in turn leads to strong electrostatic interactions according to eq 4. As the pore walls become electrified, the solvation structure of cation changes drastically: cations are displaced into pore

center and can no longer be positioned side-by-side with anions across the pore. Such a change in cation solvation structure increases the lateral separation R_{ij} between a cation and some of its solvation anions, and thus weakens their electrostatic interactions. Consequently, as the pore walls of a 1.26 nm pore become electrified, the energy gain of each cation due to its electrostatic interaction with anions, is reduced by the above weakening mechanism. Since this weakening mechanism exists in the 1.26 nm pore but not in the 1.12 nm pore, $\Delta E^{elec}_{i\rightarrow ions}(0\rightarrow\sigma)/\sigma$ tends to be less negative in the 1.26 nm pore.

The above discussions demonstrate that the scaling of EDL capacitance in pores is controlled by the screening of electrostatic interactions in different nanopores, and, more importantly, by the ion solvation structure inside nanopores and how it changes as nanopores are electrified. In particular, large capacitance can be expected if the ion solvation is weak (as in the 0.75 nm pore) or if the electrification of a pore disrupts the strong ion solvation structure inside it (as in the 1.26 nm pore). These insights have rich ramifications in the design of electrode materials and electrolytes for optimizing the capacitance of supercapacitors. Specifically, they suggest that one can optimize the capacitance of a nanopore through the manipulation of ion solvation inside the pore by tailoring the size, shape, and other chemical details of ion *pairs* for the nanopore. Such an approach goes beyond the state-of-the-art practice in which the capacitance of a nanopore is optimized by matching the size of the counterion with the nanopore width[7] and provides richer opportunities for enhancing the capacitance of supercapacitors by enabling one to exploit the vast chemical diversity of RTILs.[24]

A New Capacitor Regime. To understand the collective behavior of EDLs in supercapacitors (*e.g.*, their charging kinetics), each pore in supercapacitors is often represented by an equivalent circuit with capacitors connected in parallel and with resistors in serial.[27] Such a transmission line model has been extensively used in supercapacitor research, and it implicitly requires that, at equilibrium, the potential drop between the pore wall and the bulk electrolyte occurs *entirely* inside each pore, that is, the potential drop between the pore center and the bulk electrolyte is zero. However, we found that the electrical potential at the pore center increases from −1.10 to 0.44 V as the pore width varies from 0.75 to 1.26 nm while the total potential drop from the electrode surface to the bulk RTIL is close to 1.68 V in all pores (see Supporting Information for the potential distribution profiles in these pores). These results suggest that the transmission line model breaks down in pores studied here, and a capacitor regime qualitatively different from that in wide pores emerges. Specifically, although the charges on the pore wall are balanced by ions enclosed between the pore wall and the pore central plane, there exists a significant potential drop between the pore center and the bulk electrolyte, which has no analogy in classical capacitors. Consequently, although the pore walls and the EDLs together can still be viewed as capacitors, they can no longer be described by the transmission line model. The transmission line model will be accurate when pore width becomes large enough so that the EDLs near opposing pore walls no longer interact with each other. Since the thickness of EDL in RTILs is usually 1−3 nm, we expect that the transmission line model will be accurate in pores wider than 2−6 nm.

CONCLUSION

In summary, we studied the EDLs in nanopores filled with RTILs using MD simulations that account for the geometrical anisotropy of ions and the polarizability of pore walls. The results show that the scaling of pore capacitance exhibits a more complex behavior than previously reported, and the rich scaling behavior revealed helps settle the debate on the validity of anomalous capacitance enhancement in subnanometer pores and points to opportunities for new experimental studies. Using a newly developed mechanistic model for nanopore capacitance, we rationalized the observed scaling behaviors and showed that ion solvation structure in nanopores and its response to pore electrification play a critical role in controlling the capacitance. This insight lays the theoretical basis for optimizing pore capacitance through the manipulation of ion solvation inside nanopores by tailoring the chemical details of ion pairs for a given pore. Finally, we showed that the EDLs in nanopores filled with RTILs represent a new capacitor regime in which the transmission line model breaks down qualitatively. This result suggests that predictions of the transmission line model, which is used ubiquitously in supercapacitor research, must be carefully reassessed in the future.

METHODS

Simulations were performed using a customized MD package Gromacs.[25] The methods for enforcing electrical potential on an electrode surface and for computing electrostatic interactions are the same as that used in ref 26. Using the Faraday cage effect, the total charge on the electrode surface was controlled by fixing a corresponding amount of charges inside the electrode (denoted by the shaded regions in Figure 1) and by adjusting the number of ions inside the system to balance these charges. The length of the pores was ≥6.0 nm but varied slightly for different pores. The RTIL layers adjacent to each vertical plate are thicker than 3 nm so that bulk-like RTILs are found at positions away from the plate. The electrode was cut from a cubic lattice (lattice constant: 0.17 nm) and its atoms were

frozen. A united atom coarse grain model for the cation consisted of a 7-atom ion featuring a ring with the geometry of the native imidazolium. The anion was modeled as a 5-atom ion with the geometry of BF_4^-. The charge of each ion was located on one of its atoms as shown in Figure 1b. A background dielectric constant of 2.0 was used to account for the electronic polarization of the ions. The Lennard-Jones parameters for all atoms were the same as those of carbon.[26]

Simulations were performed in the NVT ensemble ($T = 400$ K). Each system was simulated three times using different initial configurations and consisted of an equilibrium run of 10 ns and a production run of 10 ns. The charge density of pore walls was obtained by computing the net ion charge in the middle section of each pore—entrance effects associated with pore mouth were found to be negligible at a distance greater than 1.2 nm from the mouth. The potential drop from the electrode surface to bulk RTILs was determined by solving the Poisson equation inside the system using the space charge density from the simulations.

Acknowledgment. The authors thank the Clemson-CCIT office for providing computer time. The Clemson authors acknowledge support from NSF under Grant No. CBET-0756496. R.Q. and V.M. were partially supported by an appointment to the HERE program for faculty at the Oak Ridge National Laboratory (ORNL) administered by ORISE. The authors at ORNL acknowledge the support from the Center for Nanophase Materials Sciences, which is sponsored at ORNL by the Office of Basic Energy Sciences, U.S. Department of Energy.

Supporting Information Available: Ion density distribution profiles in the 0.78, 0.84, 1.04, and 1.17 nm pores, the electrical potential distribution profiles in pores studied in this work, and the method for modeling polarizable electrodes. This material is available free of charge *via* the Internet at http://pubs.acs.org.

REFERENCES AND NOTES

1. Conway, B. E. *Electrochemical Supercapacitors*; Kluwer Academic: New York, 1999.
2. Korenblit, Y.; Rose, M.; Kockrick, E.; Borchardt, L.; Kvit, A.; Kaskel, S.; Yushin, G. High-Rate Electrochemical Capacitors Based on Ordered Mesoporous Silicon Carbide-Derived Carbon. *ACS Nano* **2010**, *4*, 1337–1344.
3. Miller, J. R.; Outlaw, R. A.; Holloway, B. C. Graphene Double-Layer Capacitor with ac Line-Filtering Performance. *Science* **2010**, *329*, 1637–1639.
4. Zhang, L. L.; Zhao, X. S. Carbon-Based Materials as Supercapacitor Electrodes. *Chem. Soc. Rev.* **2009**, *38*, 2520–2531.
5. Zhu, Y.; Murali, S.; Stoller, M. D.; Ganesh, K. J.; Cai, W.; Ferreira, P. J.; Pirkle, A.; Wallace, R. M.; Cychosz, K. A.; Thommes, M.; *et al.* Carbon-Based Supercapacitors Produced by Activation of Graphene. *Science* **2011**, *332*, 1537–1541.
6. Chmiola, J.; Yushin, G.; Gogotsi, Y.; Portet, C.; Simon, P.; Taberna, P. L. Anomalous Increase in Carbon Capacitance at Pore Sizes Less Than 1 Nanometer. *Science* **2006**, *313*, 1760–1763.
7. Largeot, C.; Portet, C.; Chmiola, J.; Taberna, P.-L.; Gogotsi, Y.; Simon, P. Relation between the Ion Size and Pore Size for an Electric Double-Layer Capacitor. *J. Am. Chem. Soc.* **2008**, *130*, 2730–2731.
8. Lin, R.; Huang, P.; Segalini, J.; Largeot, C.; Taberna, P. L.; Chmiola, J.; Gogotsi, Y.; Simon, P. Solvent Effect on the Ion Adsorption from Ionic Liquid Electrolyte into Sub-nanometer Carbon Pores. *Electrochim. Acta* **2009**, *54*, 7025–7032.
9. Centeno, T. A.; Sereda, O.; Stoeckli, F. Capacitance in Carbon Pores of 0.7 to 15 nm: A Regular Pattern. *Phys. Chem. Chem. Phys.* **2011**, *13*, 12403–12406.
10. Huang, J.; Sumpter, B. G.; Meunier, V. A Universal Model for Nanoporous Carbon Supercapacitors Applicable to Diverse Pore Regimes, Carbon Materials, and Electrolytes. *Chem.—Eur. J.* **2008**, *14*, 6614–6626.
11. Feng, G.; Qiao, R.; Huang, J. S.; Sumpter, B. G.; Meunier, V. Ion Distribution in Electrified Micropores and Its Role in the Anomalous Enhancement of Capacitance. *ACS Nano* **2010**, *4*, 2382–2390.
12. Wander, M. C. F.; Shuford, K. L. Molecular Dynamics Study of Interfacial Confinement Effects of Aqueous NaCl Brines in Nanoporous Carbon. *J. Phys. Chem. C* **2010**, *114*, 20539–20546.
13. Yang, L.; Fishbine, B. H.; Migliori, A.; Pratt, L. R. Molecular Simulation of Electric Double-Layer Capacitors Based on Carbon Nanotube Forests. *J. Am. Chem. Soc.* **2009**, *131*, 12373–12376.
14. Tanaka, A.; Iiyama, T.; Ohba, T.; Ozeki, S.; Unta, K.; Fujimori, T.; Kanoh, H.; Kaneko, K. Effect of a Quaternary Ammonium Salt on Propylene Carbonate Structure in Slit-Shape Carbon Nanopores. *J. Am. Chem. Soc.* **2010**, *132*, 2112–2113.
15. Wang, S.; Li, S.; Cao, Z.; Yan, T. Y. Molecular Dynamic Simulations of Ionic Liquids at Graphite Surface. *J. Phys. Chem. C* **2010**, *114*, 990–995.7.
16. Shim, Y.; Kim, H. J. Nanoporous Carbon Supercapacitors in an Ionic Liquid: A Computer Simulation Study. *ACS Nano* **2010**, *4*, 2345–2355.
17. Kondrat, S.; Kornyshev, A. Superionic State in Double-Layer Capacitors with Nanoporous Electrodes. *J. Phys. Condens. Matter* **2011**, *23*, 022201.
18. Kondrat, S.; Georgi, N.; Fedorov, M. V.; Kornyshev, A. A. A Superionic State in Nano-Porous Double-Layer Capacitors: Insights from Monte Carlo Simulations. *Phys. Chem. Chem. Phys.* **2011**, *13*, 11359–11366.
19. Feng, G.; Huang, J.; Sumpter, B. G.; Meunier, V.; Qiao, R. A "Counter-Charge Layer in Generalized Solvents" Framework for Electrical Double Layers in Neat and Hybrid Ionic Liquid Electrolytes. *Phys. Chem. Chem. Phys.* **2011**, *13*, 14723–14734.
20. Nanjundiah, C.; McDevitt, S. F.; Koch, V. R. Differential Capacitance Measurements in Solvent-Free Ionic Liquids at Hg and C Interfaces. *J. Electrochem. Soc.* **1997**, *144*, 3392–3397.
21. IUPAC. *Compendium of Chemical Terminology*, 2nd ed. (the "Gold Book"); McNaught, A. D., Wilkinson, A., Eds.; Blackwell Scientific Publications: Oxford, 1997.
22. This can be deduced from the ion distribution profile shown in Figure 3. Specifically, the separation between the cation density peak near one pore wall and the anion density peak near the opposite wall is 0.32 nm, which is nearly the closest approach (~0.3 nm) between the charged atoms in the anion and in the cation.
23. Tinkle, M. D.; Barlow, S. E. Image Charge Forces inside Conducting Boundaries. *J. Appl. Phys.* **2001**, *90*, 1612–1624.
24. Baldelli, S. Surface Structure at the Ionic Liquid-Electrified Metal Interface. *Acc. Chem. Res.* **2008**, *41*, 421–431.
25. Lindahl, E.; Hess, B.; van der Spoel, D. Gromacs 3.0: A Package for Molecular Simulation and Trajectory Analysis. *J. Mol. Modell.* **2001**, *7*, 306–317.
26. Feng, G.; Qiao, R.; Huang, J.; Sumpter, B. G.; Meunier, V. Atomistic Insight on the Charging Energetics in Subnanometer Pore Supercapacitors. *J. Phys. Chem. C* **2010**, *114*, 18012–18016.
27. de Levie, R. On Porous Electrodes in Electrolyte Solutions: I. Capacitance Effects. *Electrochim. Acta* **1963**, *8*, 751–780.